Journal of Applied Physics

Breaking atomic-level ordering via biaxial strain in functional oxides: A DFT study

Cite as: J. Appl. Phys. **129**, 095301 (2021); https://doi.org/10.1063/5.0039420
Submitted: 02 December 2020 . Accepted: 10 February 2021 . Published Online: 02 March 2021

Kanishk Rawat, Dillon D. Fong, and Dilpuneet S. Aidhy

AIP Publishing

Journal of Applied Physics ARTICLE scitation.org/journal/jap

Breaking atomic-level ordering via biaxial strain in functional oxides: A DFT study

Cite as: J. Appl. Phys. **129**, 095301 (2021); doi: 10.1063/5.0039420
Submitted: 2 December 2020 · Accepted: 10 February 2021 ·
Published Online: 2 March 2021

View Online Export Citation CrossMark

Kanishk Rawat,[1] Dillon D. Fong,[2] and Dilpuneet S. Aidhy[1,a)]

AFFILIATIONS

[1]Department of Mechanical Engineering, University of Wyoming, Laramie, Wyoming 82071, USA
[2]Materials Science Division, Argonne National Laboratory, Lemont, Illinois 60439, USA

[a)]**Author to whom correspondence should be addressed:** daidhy@uwyo.edu

ABSTRACT

Oxygen vacancies are found to play a crucial role in inducing many functional properties at the heterointerfaces in complex oxides. Gaining better control over the properties requires an understanding of the atomic structure of oxygen vacancies at the heterointerfaces. In this paper, we elucidate the effects of the interfacial strain on the oxygen-vacancy ordering in fluorite δ-Bi_2O_3 and perovskite $LaNiO_{2.5}$ using first-principles calculations. By applying biaxial strains, we find that the ⟨110⟩−⟨111⟩ oxygen vacancy order in δ-Bi_2O_3 is broken, resulting in a faster diffusion of oxygen ions. Similarly, the biaxial strain is used to leverage both ordered and disordered arrangements of vacancies in $LaNiO_{2.5}$. Besides the vacancy order, we find that the biaxial strain can also be used to break the cation order in $Gd_2Ti_2O_7$, where Gd and Ti antisites can be created on the cation sublattice, which leads to enhanced radiation tolerance and higher oxygen diffusivity. These results indicate that the biaxial strain that is commonly present at heterointerfaces can be used to gain control over both ordered and disordered arrangements of defects, potentially opening new opportunities to functionalize complex oxides.

I. INTRODUCTION

Oxygen vacancies are critical for inducing various functional properties in ceramic oxides. One of the most common examples is the oxygen ion transport in solid oxide fuel cells where oxygen atoms diffuse via the vacancy mechanism.[1–3] The oxygen vacancies are specifically created in solid electrolytes such as zirconia and ceria by adding trivalent dopants, to induce oxygen diffusion. Similarly, it has been found that the presence of oxygen vacancies can lead to a change in the oxidation state of metal atoms, thereby creating charge carriers that can induce metal–insulator transition (MIT). This phenomenon has been observed in the reduction of $LaNiO_3$ to $LaNiO_{2.5}$ due to oxygen vacancies forming Ni^{2+} ions that promote MIT.[4,5] Oxygen vacancies are held responsible for the self-healing properties of pyrochlore oxides (e.g., $Gd_2Ti_2O_7$) that are potential candidates for storing nuclear waste.[3,6–8] Oxygen vacancies have also been considered one of the key reasons for the emergence of novel properties in thin-film heterointerfacial oxides.[9–11]

Quite often, it has been observed that oxygen vacancies can arrange themselves to form ordered networks in a crystal lattice that limit material properties. For example, above 727 °C, δ-Bi_2O_3 has the highest oxygen conductivity among various fluorite oxides used as solid electrolytes in solid oxide fuel cells. However, when doped with lanthanides to stabilize the fluorite phase at the desirable temperature of 500 °C, the vacancies order in a ⟨110⟩−⟨111⟩ network, leading to a dramatic loss of ionic conductivity.[12–16] Similarly, oxygen vacancy ordering has also been found to affect electronic conductivity in $LaNiO_{3-x}$. In $LaNiO_{2.75}$, a higher electronic conductivity and an MIT are observed in the presence of an ordered arrangement of oxygen vacancies as compared to lower conductivity and no observable MIT in the presence of a disordered arrangement of oxygen vacancies.[17] Similarly, increasing the amount of oxygen vacancy disorders can decrease the electronic conductivity of paramagnetic $SmNiO_3$.[18] Besides oxygen vacancies, the ordering of atoms can also affect material properties. In particular, pyrochlore oxides (with the chemical formula $A_2B_2O_7$) have an ordered arrangement of A^{3+} and B^{4+} cations. The self-healing property of pyrochlores under irradiation is anchored in the ability of A and B cations to easily switch their sites, i.e., forming antisites on the cation sublattice.[3,19] Consequently, the oxygen vacancies that are locked due to A and B ordering are unlocked when the two cations switch sites, thereby leading to faster oxygen diffusion.

Thus, the ordering of both oxygen vacancies and cations can determine the functional properties of ceramic oxides: breaking this order can be a powerful means of controlling functionality.

Due to the vibrant interest shown by researchers in heterostructures and the properties of materials at the interfaces of thin films,[20–23] the role of interfacial strain in defect ordering is an attractive parameter to investigate. In recent years, researchers have leveraged interfacial strain to gain control over oxygen vacancies. For example, tensile strain in fluorite oxides is found to have lower oxygen vacancy migration barriers, affecting the kinetics of oxygen diffusion, thereby leading to faster oxygen conductivity.[3,24–26] Similarly, the thermodynamics of oxygen vacancies, i.e., the formation energy of oxygen vacancies, has also been correlated with interfacial strain to manipulate the oxygen vacancy concentration near the interfaces.[9,27–32] For instance, density functional theory (DFT) calculations have shown that strain can be used to increase the concentration of oxygen vacancies in $CaMnO_3$[27] by lowering their formation energies. Similarly, DFT calculations have shown that in $SrCoO_{3-\delta}$ thin films, tensile strain results in lower formation energies of equatorial oxygen vacancies (i.e., vacancies in the plane of biaxial strain) compared with apical vacancies (i.e., vacancies that are perpendicular to the plane of biaxial strain).[31] Thus, interfacial strain constitutes a common parameter through which the energetics of oxygen vacancies can be controlled. In this work, we show that interfacial strain can be used to break the ordering, of both oxygen vacancies and cations, in oxide materials. In particular, we show that tensile strain can (1) break the ⟨110⟩−⟨111⟩ oxygen vacancy order in fluorite δ-Bi_2O_3, (2) allow for the creation of a metastable vacancy disorder in perovskite $LaNiO_{2.5}$, (3) and break the A and B cation order in $Gd_2Ti_2O_7$ pyrochlore. This ability to break the order via strain opens a new pathway to control the energetics of oxygen vacancies and prevent the degradation of properties in heterointerfacial oxides. More importantly, a correlation between strain and atomic order is developed in this work.

II. CRYSTAL STRUCTURES

A. δ-Bi_2O_3

Figure 1(a) shows a 2 × 2 × 2 supercell of δ-Bi_2O_3, which is an oxygen deficient fluorite-based structure. The space group of δ-Bi_2O_3 is $Fm\bar{3}$ (No. 202),[33] and the lattice constant is 11.288 Å.[33] In comparison with an ideal fluorite structure (such as in CeO_2) that has eight oxygen atoms in its unit cell, δ-Bi_2O_3 has six oxygen atoms and two structural vacancies. The lack of two oxygen atoms is accounted for by the +3 valence state of Bi. Previous works have shown that the vacancies form an ordered network in the ⟨110⟩−⟨111⟩ fashion, which requires a 2 × 2 × 2 supercell for a complete description of the structure. The ⟨110⟩−⟨111⟩ ordered vacancy network has been observed from neutron-scattering experiments and is supported by DFT calculations.[33,34]

B. $LaNiO_{2.5}$

The rare-earth nickelate $LaNiO_3$ has a rhombohedral distorted perovskite-based structure. It has an $R\bar{3}c$ space group (No. 167), a lattice constant of 5.250 Å, and α = 61.4°.[35] Oxygen deficient $LaNiO_{2.5}$ exists in a monoclinic phase, with the c2/c space group (No. 15)[35,36] and with lattice constants a = 7.830 Å, b = 7.800 Å, c = 7.740 Å, and β = 93.7°.[36] However, $LaNiO_{2.5}$ can be stabilized in a pseudocubic form when grown as a thin film. Recently, Tung *et al.*[4] grew $LaNiO_{2.5}$ on $SrTiO_3$ and proposed a pseudocubic structure of $LaNiO_{2.5}$ (called structure A[4] as per its nomenclature), shown in Fig. 1(b). Previous studies have described the structure of oxygen deficient $LaNiO_{2.5}$ as similar to that of $LaNiO_3$ but with Ni-O_4 square planar coordination in the ⟨110⟩ direction,[37,38] alternating with Ni-O_6 octahedra.

C. $Gd_2Ti_2O_7$

$Gd_2Ti_2O_7$ has a pyrochlore structure with space group $Fd\bar{3}m$ (No. 227).[3] Its structure can be described as a 2 × 2 × 2 supercell of

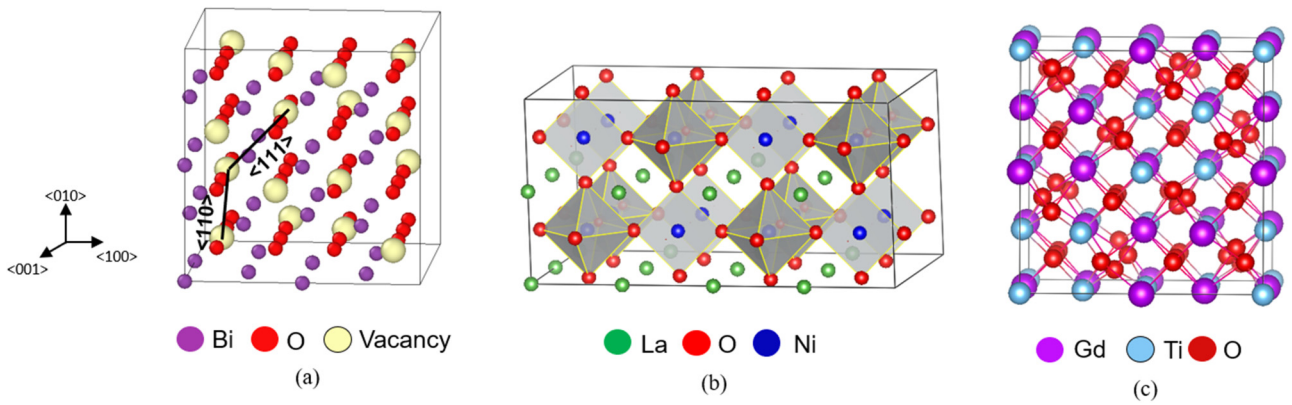

FIG. 1. (a) A 2 × 2 × 2 δ-Bi_2O_3 structure with ⟨110⟩−⟨111⟩ ordered oxygen vacancies. (b) A 2 × 4 × 2 supercell of $LaNiO_{2.5}$ showing structure A where the square planars are represented by the lighter gray shade, whereas the octahedra are represented by the darker gray shade. See text for a description of structure A. (c) An ordered 1 × 1 × 1 $Gd_2Ti_2O_7$ pyrochlore structure.

a fluorite structure. Due to +3 and +4 valencies of Gd and Ti, respectively, each 1/8th unit cell contains one structural oxygen vacancy. The cubic lattice parameter of $Gd_2Ti_2O_7$ is 10.260Å.[3] Figure 1(c) shows the ideal pyrochlore structure where Gd and Ti cations are ordered, i.e., they occupy *16c* and *16d* Wyckoff sites, respectively. The oxygen atoms occupy *8b* and *48f* sites, whereas the vacancies occupy *8a* sites. In the disordered structure, both cations are randomly distributed on the cation sublattice, and oxygen atoms and vacancies are randomly distributed on the anion sublattice.

III. METHODOLOGY

To investigate the effect of biaxial strain on these structures, spin-polarized DFT calculations are performed using the Vienna *ab initio* Simulation Package (VASP).[39] In all calculations, the Perdew–Burke–Ernzerhof (PBE) form of the generalized gradient approximation (GGA)[40] for the exchange–correlation functionals is used.

For δ-Bi_2O_3, a plane wave energy cutoff of 500 eV and a $3\times3\times3$ Monkhorst–Pack[41] *k-point* sampling mesh are used for the $2\times2\times2$ defect fluorite supercell containing 80 atoms. The total energy is converged with a 1×10^{-4} eV tolerance. The ⟨110⟩−⟨111⟩ δ-Bi_2O_3 structure is derived from a previous work[33] and is found to have a lattice constant of 11.196Å. In this work, we also consider other vacancy-ordered structures, i.e., vacancies ordered in ⟨100⟩, ⟨110⟩, and ⟨111⟩ directions. In these three structures, a $1\times1\times1$ unit cell is used, because the ordering in these structures can be described by a 10-atom unit cell. In addition to the vacancy-ordered structures, the disordered structures of δ-Bi_2O_3, i.e., containing the random positioning of oxygen vacancies, are also considered. For the three disordered structures, named D1, D2, and D3, $2\times2\times2$ supercells containing 80 atoms are used. Although the disordering of the vacancies is done by hand, which may not represent complete randomness in the supercell, our calculations reveal that as long as the strictly ordered structure is broken, the presence of some level of randomness destabilizes the ordered structure under biaxial strain. Consequently, the disordered structures become more stable, which leads to a change in the atomic-level properties.

For all $LaNiO_3$ and $LaNiO_{2.5}$ calculations, a plane wave energy cutoff of 520 eV is used with a $4\times2\times4$ *k-point* sampling mesh for a $2\times4\times2$ pseudocubic supercell containing 80 atoms. The convergence criteria used is the same as that of δ-Bi_2O_3, i.e., the total energy is converged with a tolerance of 0.0001 eV. $LaNiO_3$ is modeled in a pseudocubic perovskite-based structure. Eight oxygen vacancies are introduced in the 80 atom system to obtain $LaNiO_{2.5}$. As mentioned previously, due to the ordering of oxygen vacancies in $LaNiO_{2.5}$, there are alternating patterns of octahedral and square-planar coordinated Ni sites. While Tung *et al.*[4] presented two structures of $LaNiO_{2.5}$ (i.e., structures A and B as per their nomenclature and renamed o1 and o2, respectively, in this work), we observed that other ordered structures could have lower energies. Therefore, we created ten other ordered structures of $LaNiO_{2.5}$, as shown in Fig. S1 in the supplementary material section; these structures are named o3, o4, o5, and so on. In addition, we consider five structures with disordered vacancies (named d1, d2, d3, and so on), as shown in Fig. S1 in the supplementary material section. The energies of the oxygen-deficient cubic structures are evaluated at various biaxial strains. Under the assumption that the thin films are grown on cubic perovskite substrates such as $SrTiO_3$, the structures are relaxed at the +2% strain, while the cell volume and shape are constrained. The total energies of the structures are compared to ascertain the stability of various vacancy-ordered structures under different strain conditions.

For $Gd_2Ti_2O_7$, a plane wave energy cutoff of 500 eV is used with a $3\times3\times3$ *k-point* sampling mesh for a $2\times2\times2$ supercell containing 88 atoms. The same convergence criteria described above are used. The structure of $Gd_2Ti_2O_7$ with a disordered arrangement of cations is taken from a previous work.[3]

When biaxial strain is applied in a given plane, the height of the unit cell in the out-of-plane axis changes according to the Poisson's ratio. We calculate the c-axis lattice constant by constructing an energy vs volume curve by gradually varying the length of the supercell in the c-axis for a fixed x–y biaxial strain; the minimum in the curve is the obtained c-axis constant. These calculations are performed for both x–y biaxial strains (i.e., −2% and +2%) for all δ-Bi_2O_3, $LaNiO_{2.5}$, and $Gd_2Ti_2O_7$ ordered and disordered structures. An example of the energy vs volume curve for an o4 structure of $LaNiO_{2.5}$ is shown in Fig. S2 in the supplementary material section. It shows the energies of the structures as the c-axis length is varied. We find that when a +2% tensile strain is applied, the c axis relaxes from 3.832 Å to 3.680 Å, as shown in Fig. S2 in the supplementary material. In order to validate this method, we also compute the c-axis lattice constant for bulk $LaNiO_3$ under the +2% biaxial strain and find it to be 3.800 Å, which is in agreement with that in the previous literature.[4,42]

Finally, we have performed molecular dynamics (MD) simulations to understand oxygen diffusion in δ-Bi_2O_3 and $Gd_2Ti_2O_7$. The simulations are performed using the Large-scale Atomic Molecular/Massively Parallel Simulator (LAMMPS) code.[43] The interatomic potential and the MD simulation parameters for δ-Bi_2O_3 such as time step, temperature, etc., are identical to previous works.[33,44] The simulations were performed using a time step of 0.5 fs up to a total of 200 000 MD steps at 1000 K. Similarly, for $Gd_2Ti_2O_7$, the interatomic potential is also derived from previous works.[3,19] The MD simulations are performed in a biaxially strained supercell, where the supercell is strained in the x and y directions, while the z axis is allowed to relax by fixing the volume of the supercell. Mean square displacement (MSD) is used to measure oxygen diffusion given by the following equation:

$$\mathrm{MSD} = \frac{1}{N}\sum\left(r^i_{t+\Delta t} + r^i_t\right)^2, \tag{1}$$

where r^i_t is the ion's position at time t and N is the total number of diffusing ions. The diffusion constant D is related to MSD by the relation $\mathrm{MSD} = 6Dt$.[33]

IV. RESULTS

A. δ-Bi_2O_3

Figure 2 shows a comparison of system energies among four ordered and three disordered structures of δ-Bi_2O_3. As mentioned

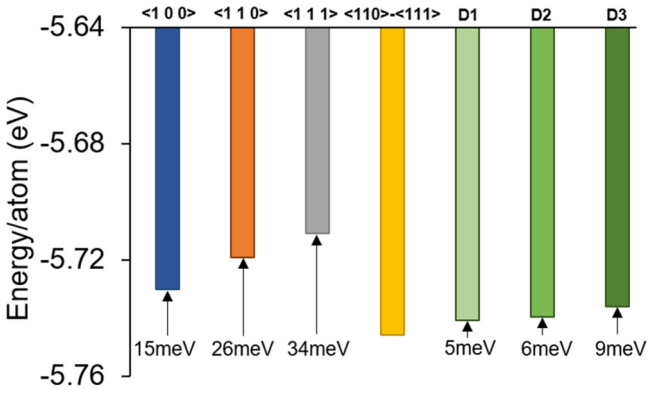

FIG. 2. Comparison of the system stability among various ordered and disordered structures in δ-Bi_2O_3 at 0% strain. The ⟨110⟩−⟨111⟩ structure is the lowest energy structure, in agreement with that in previous work.[33]

above, in the ordered structures, the vacancies are ordered in the ⟨100⟩, ⟨110⟩, ⟨111⟩, and ⟨110⟩−⟨111⟩ directions, whereas in the disordered structures, the vacancies are randomly distributed on the oxygen sublattice. In agreement with a previous work,[33] we find that the ⟨110⟩−⟨111⟩ ordered structure is the lowest energy structure, as shown in Fig. 2. The optimized lattice constant of 11.198 Å is also in good agreement with that in the previous DFT works.[13,33]

For oxygen vacancies ordered in the ⟨100⟩ and ⟨110⟩ directions, the vacancies can lie in either the plane of the biaxial strain or perpendicular to it. Figure 3(a) shows the possible scenarios with unit cells of vacancies in the ⟨100⟩, ⟨110⟩, and ⟨111⟩ directions and the plane of the biaxial strain indicated by the blue dotted lines. The directions of the applied strain corresponding to the dotted line are shown for ⟨100⟩_xy, represented by the arrows. Since the ⟨100⟩ vacancies lie in the x–y plane, if biaxial strain is applied in the x and y directions, the vacancies are in the plane of the strain, represented by ⟨100⟩_xy. If the biaxial strain is applied in the y–z plane, the ⟨100⟩ vacancies are perpendicular to the plane of the biaxial strain and the orientation is represented by ⟨100⟩_yz. Similarly, in the structure with ⟨110⟩ ordering, when biaxial strain is applied in the x and y directions (⟨110⟩_xy), the vacancies lie in the plane, and when the strain is applied in the y and z directions, the vacancies lie perpendicular to the plane of the strain (⟨110⟩_yz). In the ⟨111⟩ ordered structure, the plane of the biaxial strain is independent of the orientation of vacancies; therefore, the system is strained only in the y–z plane, as shown in Fig. 3(a).

The energies for all ordered and disordered structures under different biaxial strains are compared in Fig. 3(b). Under both 0% and −2% strains, the ⟨110⟩−⟨111⟩ ordered structure has the lowest energy. However, under a +2% strain, the stability changes and the disordered structure, D1, has the lowest energy. Additionally, the disordered structures D2 and D3 have lower energies than the ⟨110⟩−⟨111⟩ ordered structure at the +2% strain.

It is interesting to note that while the stability of the structures changes from ⟨110⟩−⟨111⟩ to disordered as the strain changes from −2% to +2%, the other three ordered structures, i.e., ⟨100⟩, ⟨110⟩, and ⟨111⟩, remain higher in energy across all strain ranges. However, within these three ordered structures, their relative stability does change. While at 0% strain, the ⟨100⟩ structure has the lowest energy, followed by ⟨110⟩ and ⟨111⟩ structures, under 2% strain, the ⟨110⟩_yz structure has the lowest energy followed by ⟨110⟩_xy, ⟨111⟩, ⟨100⟩_xy, and ⟨100⟩_yz structures. A similar trend is observed when the samples are under tensile strain. These results indicate that (1) biaxial strain can be used to break the ordered arrangement of vacancies to induce disorder in the anion sublattice and (2) different ordered arrangements can be stabilized at different amounts of biaxial strains.

The effect of change in the ordering of the vacancies on oxygen diffusivity is captured in MD simulations. Previously, Aidhy *et al.*[33] showed that under 0% strain, oxygen atoms do not diffuse once the structure is locked in a ⟨110⟩−⟨111⟩ ordered arrangement of vacancies. The MSD for the ⟨110⟩−⟨111⟩ structure is reproduced in Fig. 4(a); it shows a plateau indicating that no oxygen diffusion takes place and the vacancies remain ordered throughout the length of the simulation.

Based on the DFT results that under tensile strain, the disordered structures could be relatively more stable than the ordered structures, it is hypothesized that once the ⟨110⟩−⟨111⟩ ordered network of vacancies is broken by applying tensile strain, the oxygen vacancies will continue to diffuse. We test this hypothesis by performing MD simulations on ⟨110⟩−⟨111⟩ ordered and two disordered (D1 and D2) structures, all under a 6% biaxial tensile strain. A higher tensile strain is chosen in order to allow appreciable oxygen diffusion on a limited MD time scale. Figure 4(b) shows the MSD in the three structures. Instead of a plateau, continuous oxygen diffusion is observed in all three structures, indicating that the ⟨110⟩−⟨111⟩ ordered network, which is otherwise stable under the 0% strain, is now broken, and the oxygen vacancies diffuse throughout the duration of the simulation. Identical MSD slopes are observed for the two disordered structures, indicating that all three structures have disordered vacancies leading to high oxygen diffusion. This is indicative of the fact that biaxial strain is affecting the structure and the diffusivity of the oxygen atoms. It is to be noted that while the DFT results provide the stability of the structures at 0 K, the MD simulations performed at elevated temperatures validate the prediction that the ordered network of vacancies is broken under biaxial strain [Fig. 4(b)].

An additional benefit of applying tensile strain is that it lowers the migration barriers of oxygen diffusion. Various previous studies have shown that tensile strain reduces migration barriers, thereby increasing oxygen diffusivity.[24,45–50] These calculations now show that tensile strain can also help unlock the ordered network, thereby further contributing to easier oxygen diffusion.

B. $LaNiO_{2.5}$

While performing DFT calculations, Tung *et al.*[4] considered two structures of $LaNiO_{2.5}$ distinguished by the ordering of oxygen vacancies. Their supercell consisted of $LaNiO_{2.5}$ interfaced with $SrTiO_3$. Due to a lattice mismatch of +2% between the two materials, they applied a +2% biaxial strain on $LaNiO_{2.5}$. After relaxation, they found that structure A had a lower energy than structure B. Our calculations reproduce their observations. A comparison of

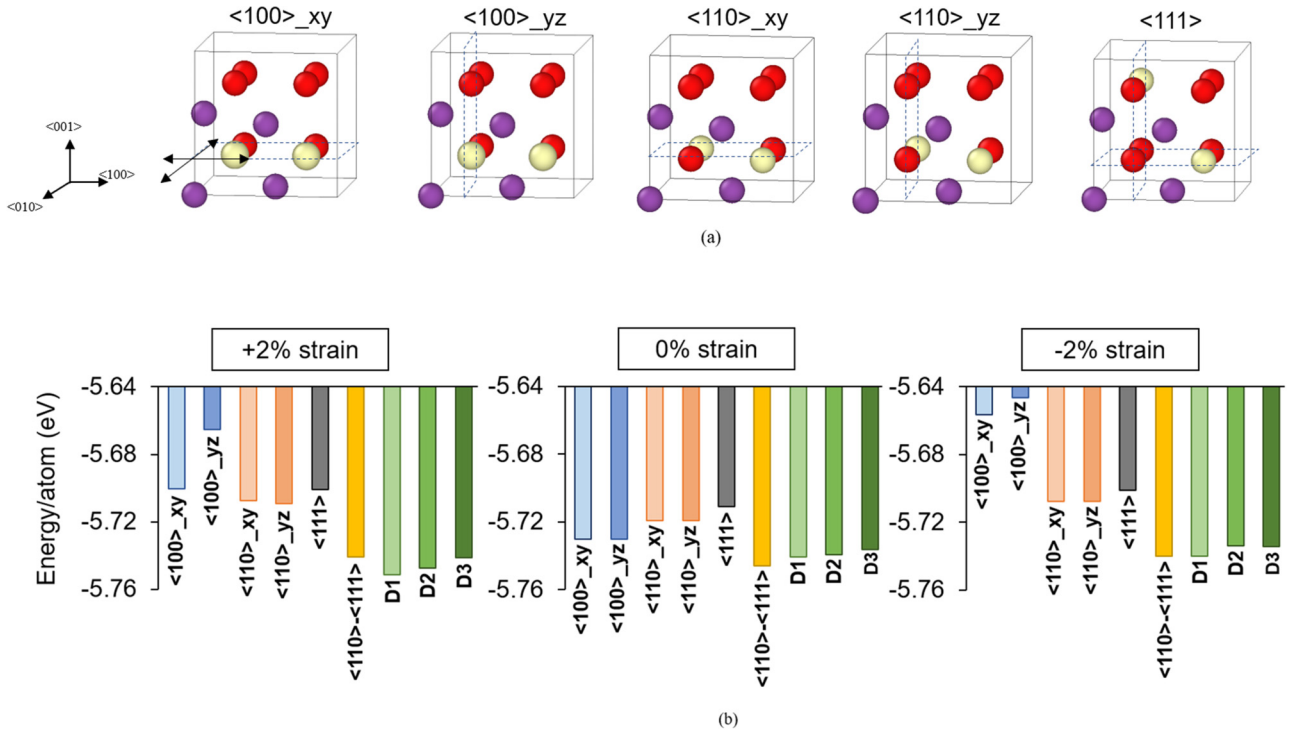

FIG. 3. (a) 1 × 1 × 1 unit cells of ⟨100⟩, ⟨110⟩, and ⟨111⟩ vacancy-ordered structures showing planes of an applied biaxial strain with Bi atoms (purple), O atoms (red) and oxygen vacancies (white). The planes in which the biaxial strain is applied with respect to the vacancies are highlighted in the unit cells (b) Comparison of system energies per atom of ordered and disordered structures at +2% biaxial strain, 0% strain, and −2% biaxial strain.

system energies of the two structures is shown in Fig. 5(a). In this work, we relabel their structures A and B as o1 and o2, respectively.

We have considered other ordered and disordered structures to understand the effect of biaxial strain on the ordering/disordering of vacancies. It is hypothesized that varying the biaxial strain can lead to a change in the oxygen vacancy pattern, thereby leading to a change in the stability of the structures. In particular, we have considered twelve ordered and five disordered structures. These structures are schematically shown in Fig. S1 in the supplementary material section. Three biaxial strain conditions are considered, i.e., +2%, 0%, and −2%. The tensile strain (i.e., +2%) corresponds to the lattice constant of $SrTiO_3$ applied to pseudocubic $LaNiO_{2.5}$. As discussed in Sec. III, the c-axis lattice constant is calculated corresponding to each strain condition for each of the seventeen structures. The relaxed c-axis lattice constants for all structures are given in Table I.

Figure 5 shows a comparison of energies of 17 structures under three different strain conditions. While o1 has a lower energy than o2 under the +2% strain, as shown in Fig. 5(a), their relative stability changes under the 0% strain, as shown in Fig. 5(b). Their energy difference further increases at −2%, as shown in Fig. 5(c), indicating that the o2 structure is expected to be more stable than o1 under compressive strain. This result indicates that the vacancy ordering changes with biaxial strain in $LaNiO_{2.5}$.

While o1 is relatively more stable than o2 under a +2% strain, we find that it is not the lowest energy structure. Instead, we find that o8 is the lowest energy structure, which has 7 meV/atom lower energy than o1. Furthermore, three other structures, i.e., o3, o4, and o11, have 6 meV/atom lower energies than o1. These three structures have identical energies despite a different arrangement of oxygen vacancies, as shown in Fig. S1 in the supplementary material section. It is also observed that all of the disordered structures, i.e., d1–d5, have higher energies under the +2% strain. Thus, based on Fig. 5(a), ordered vacancies can be expected in $LaNiO_{2.5}$ when grown on $SrTiO_3$.

In contrast, under 0% strain, we find that the stability of the structures changes from ordered to disordered. Figure 5(b) shows that d3 is the lowest energy structure among all, followed by d4. The ordered structure, i.e., o8, is the third most stable structure. While the other three disordered structures are significantly higher in energy than ordered structures, Fig. 5(b) illustrates that disordered vacancies can be expected in $LaNiO_{2.5}$ under 0% strain. The stability of disordered vacancies over ordered vacancies has been observed experimentally by Hirai *et al.*[51] in the $SrFeO_{2.5}/DyScO_3$ interface. Using high-angle annular dark-field scanning transmission electron microscopy (HAADF-STEM), it was observed that the vacancies were completely disordered up to 5 nm thickness from the interface. As the strain relaxed at higher film thicknesses,

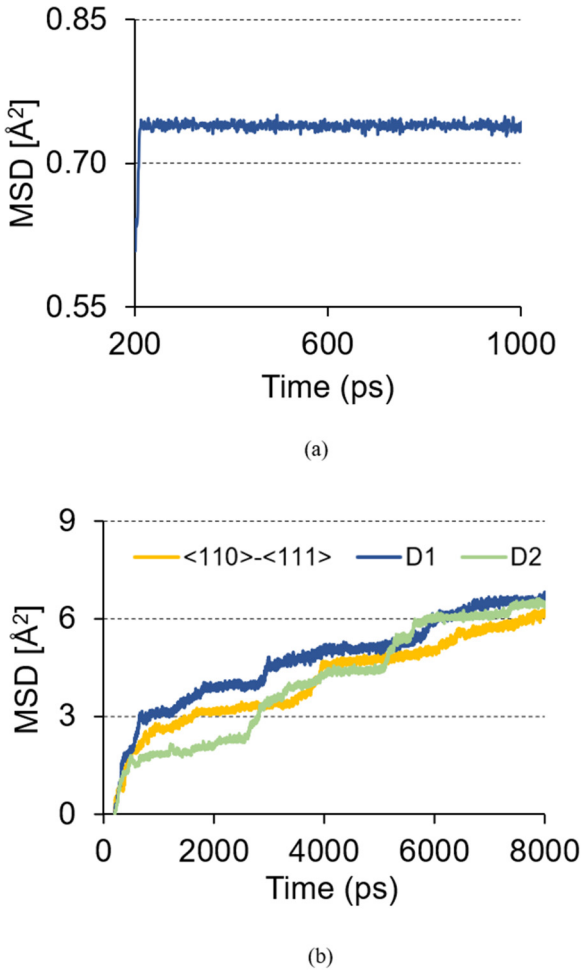

FIG. 4. Mean-square displacement of oxygen in the δ-Bi_2O_3 structure at (a) 0% strain in the ⟨110⟩−⟨111⟩ ordered structure and (b) 6% strain in ordered and disordered structures.

the authors showed the transition from a disordered to an ordered arrangement of vacancies. Thus, our DFT predictions qualitatively agree with the experimental observation, i.e., strain can affect the order/disorder arrangement of vacancies.

Finally, under a −2% compressive strain, we find that the o2 ordered structure is the most stable structure, sequentially followed by o7, o10, and d3, as shown in Fig. 5(c). The change in stability from ordered to disordered and back to ordered vacancy structures from +2% to 0% to −2%, respectively, indicates that the stability of the vacancy structures depends on the amount of strain applied, which can, in turn, be correlated to the chemical expansion of the oxygen vacancies. Previous works have shown that an oxygen vacancy generally occupies a larger volume than an oxygen atom, leading to chemical expansion in the material.[9,45–53] Here, because the vacancies are ordered in different orientations, the biaxial strain can affect the chemical expansion and hence the relative stability of the structures. This could possibly be a reason for the stability of different structures under different amounts of strain, as shown in Figs. 5(a)–5(c).

C. $Gd_2Ti_2O_7$

Pyrochlore oxides have shown diverse electronic and atomic properties such as the MIT, topological insulators, fast oxygen-ion transport, and high radiation resistance for nuclear waste-storage applications.[8,19,54] However, gaining control over these properties in bulk pyrochlores has remained an open challenge due to the lack of simpler methods to stabilize the specific "disordered" structure in these materials needed to induce these properties.

Based on the DFT results obtained in δ-Bi_2O_3 and $LaNiO_{2.5}$, we explore the possibility of changing the cation ordering in the pyrochlore structure $Gd_2Ti_2O_7$. It was previously shown that cation disorder could be achieved by applying volumetric strain[3] where a disordered structure was found to be more stable than an ordered one under higher tensile strains. In this work, we focus on the effect of biaxial strain on the relative stability of ordered and disordered structures. The disordered structure is taken from a previous work.[3] The energy vs volume curve is plotted for the two structures, as shown in Fig. 6(a). For each amount of biaxial strain, the

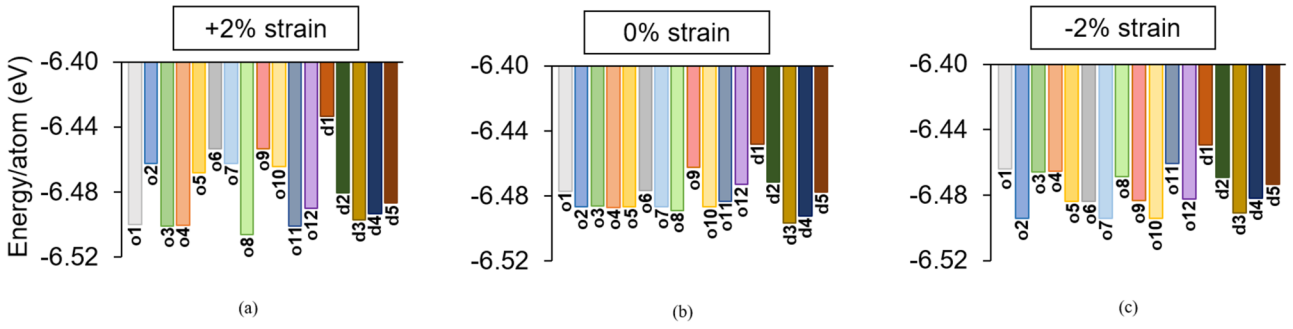

FIG. 5. Comparison of system energies per atom among various ordered and disordered $LaNiO_{2.5}$ structures at (a) +2%, (b) 0%, and (c) −2% biaxial strains.

TABLE I. Relaxed c-axis lattice constants (in Å) for all ordered and disordered $LaNiO_{2.5}$ structures under +2% (x = y = 7.850 Å), 0%, and −2% (x = y = 7.500 Å) biaxial strains.

Strain	o1	o2	o3	o4	o5	o6	o7	o8	o9	o10	o11	o12
+2%	3.650	3.830	3.680	3.680	3.810	3.810	3.840	3.670	3.840	3.840	3.660	3.610
0%	3.830	3.830	3.830	3.830	3.830	3.830	3.830	3.830	3.830	3.830	3.830	3.830
−2%	3.750	3.920	3.800	3.770	3.910	3.910	3.910	3.760	3.960	3.950	3.760	3.890
Strain	d1	d2	d3	d4	d5							
+2%	3.770	3.800	3.860	3.820	3.825							
0%	3.830	3.830	3.830	3.830	3.830							
−2%	3.900	4.000	3.990	4.000	3.970							

c-axis lattice constant is uniquely determined, as discussed in Sec. III. We find that the stability changes from ordered to disordered at a volume of 1150 $Å^3$. At the crossover point, the ordered structure is under a tensile strain of 6%, whereas the disordered structure is under a compressive strain of 4%. In the disordered structure, Gd and Ti atoms occupy antisites on the cation sublattice. As a result, Gd and Ti are not restricted to *16a* and *16b* Wyckoff sites. The oxygen atoms and vacancies are also not restricted to their corresponding *8b* and *48f*, and *8a* Wyckoff sites, respectively. As a result, the oxygen vacancies are unlocked. These calculations demonstrate that biaxial tensile strain can disorder the cation sublattice in $Gd_2Ti_2O_7$.

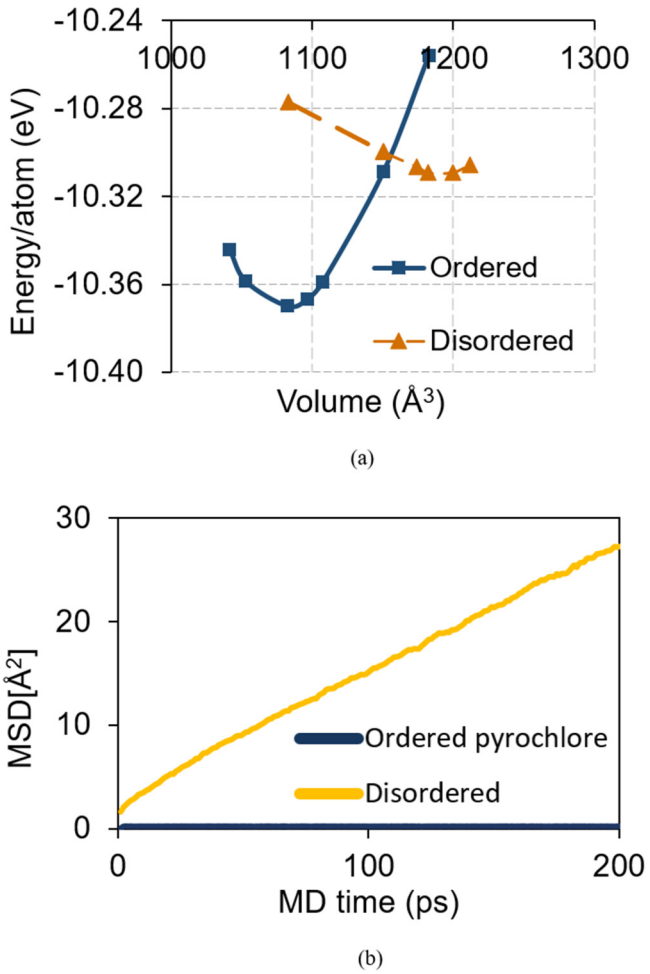

FIG. 6. (a) Comparison of system energy per atom between the ordered and the disordered structures as a function of volume from DFT calculations. (b) MSD of oxygen in ordered and disordered $Gd_2Ti_2O_7$ from MD simulations.

The unlocking of the oxygen vacancies is observed in their diffusivity behavior. Figure 6(b) shows a comparison of oxygen MSD in the ordered and disordered structures of $Gd_2Ti_2O_7$. While significant oxygen diffusion is observed in the disordered structure, no diffusion is observed in the ordered structure. The lack of oxygen diffusion is due to higher oxygen migration barriers in the ordered structure compared with lower barriers in the disordered one. These diffusivity results are consistent with those of previous works.[3,19]

VI. DISCUSSION

A. δ-Bi_2O_3

The breaking of the ordered arrangement of oxygen vacancies in δ-Bi_2O_3 via biaxial strain opens an opportunity to achieve higher oxygen-ion conductivity. While δ-Bi_2O_3 has the highest oxygen conductivity among known fluorite-based oxides, its conductivity is significantly lower at practically desirable temperatures of 500 °C because of the phase transformation from a delta phase to a monoclinic one. While the addition of trivalent dopants can stabilize the delta phase at lower temperatures, the conductivity still decreases due to the decrease in the overall cation polarizability of dopants. Note that one of the main reasons for the high conductivity of δ-Bi_2O_3 is the presence of $6s^2$ lone pair electrons in Bi, which lends high polarizability.[1,2,50,55,56] The addition of low polarizable trivalent dopants leads to a decrease in the overall cation polarizability, and hence, oxygen conductivity. Since the addition of trivalent doping is necessary to stabilize the material at relevant temperatures, the resulting loss in conductivity due to ordering of the vacancies is undesirable. The observations in this paper show that tensile interfacial strain can be used to break vacancy ordering. The disordered structures exhibit lower energies at 2% tensile strain, signifying thermodynamic stability over the ordered structure. This is supported by the MSD results, which show that while there is limited diffusion at 0% strain, significant diffusion is observed in both ordered and disordered systems under tensile strain. Thus, the

breaking of the ordered structures opens a door to nullify the loss of conductivity due to the addition of dopants.

B. $LaNiO_{2.5}$

Recently, Golalikhani *et al.*[5] showed that oxygen vacancies play a critical role in the MIT in ultrathin $LaNiO_3$ films. Using x-ray absorption spectroscopy, they detected the presence of oxygen vacancies in $LaNiO_3$ thin films. The presence of oxygen vacancies was suggested to be the cause behind the insulating behavior of ultrathin $LaNiO_3$ thin films grown on $LaAlO_3$ substrates. Tung *et al.*[4] performed DFT calculations in a $LaNiO_3$ thin film grown on $SrTiO_3$. They found that thin films are necessary to cause transformation from $LaNiO_3$ to oxygen-deficient $LaNiO_{2.5}$. They proposed two vacancy ordered structures for $LaNiO_{2.5}$. In this work, we advance the understanding and propose that both ordered and disordered arrangement of vacancies can be achieved via interfacial strain. Our results for $LaNiO_{2.5}$ indicate that at 0% strain, the disordered structure is thermodynamically stable. However, when the system is strained under both compressive and tensile conditions, different ordered systems become thermodynamically stable. Although our results show relative stability among a select group of possible orderings in the material, we propose that interfacial strain can be used as an external factor to alter vacancy ordering. This opens up pathways to grow $LaNiO_{2.5}$ on various substrates such as $LaAlO_3$ or $SrTiO_3$ and control the ordering of oxygen vacancies. As a result, this understanding opens up a possibility to induce newer functionalities in $LaNiO_{2.5}$.

Nord *et al.*[57] observed a change in the structure of $La_{0.7}Sr_{0.3}MnO_3$ (LSMO) thin films when grown on $SrTiO_3$. The LSMO thin films were subjected to a 1.2% tensile strain resulting from the smaller lattice constant of LSMO (3.876 Å) compared with $SrTiO_3$ (3.925 Å). With the combined results from DFT calculations and experiments, they found the presence of a brownmillerite phase with disordered oxygen vacancies existing 3 nm into the thin film from the interface. These examples support our prediction that strain can be potentially used to achieve an order/disorder arrangement of oxygen vacancies near the interface.

C. $Gd_2Ti_2O_7$

Previous work by Aidhy *et al.*[3] showed that the cation ordering of Gd and Ti atoms could be disrupted by the application of volumetric strain. In this work, we show that biaxial strain can also break cation ordering. This observation opens up a possibility to create cation antisites in pyrochlore thin films. Evidence of cation disorder has been recently presented in $Ho_2Ti_2O_7$ pyrochlore thin films grown on yttria stabilized zirconia.[58] Due to the lattice parameter mismatch between the two materials, a 2% strain in the thin film was observed. A large number of antisites near the interface, i.e., Ti sites on Ho sites and vice versa, were also observed. Similarly, Yang *et al.*[54] reported the presence of Bi_{Ir} antisite defects in $Bi_2Ir_2O_7$ thin films grown on YSZ. The disordering of cations due to tensile strain observed in our work is consistent with these recent results. Thus, imparting tensile strain pyrochlore as thin films carries an opportunity to affect functional properties by lowering the cation antisite energies and unlocking oxygen vacancies for fast ion diffusion.

VII. CONCLUSION

We have used biaxial strain to disrupt oxygen vacancy ordering in fluorite-based oxide δ-Bi_2O_3 and rare earth nickelate $LaNiO_{2.5}$, and cation ordering in pyrochlore $Gd_2Ti_2O_7$. With a combination of DFT and MD simulations, we show that the ordered arrangement of oxygen vacancies in δ-Bi_2O_3 can be broken via interfacial strain, thereby leading to faster oxygen diffusion. In $LaNiO_{2.5}$, we show that by varying biaxial strain, both ordered and disordered arrangement of vacancies could be achieved. Finally, we show that the ordered arrangement of cations in a pyrochlore structure could also be broken by biaxial strain. Collectively, these results indicate that biaxial strain present at the interfaces could be used as a controlling knob to affect defect energetics and potentially unravel interesting functional properties in oxide thin films.

SUPPLEMENTARY MATERIAL

See the supplementary material for the ordered and disordered $LaNiO_{2.5}$ structures with the position of oxygen vacancies along with the example of energy-volume curve used to determine relaxed c-axis constants.

ACKNOWLEDGMENTS

K.R. and D.S.A. acknowledge support by the National Science Foundation under Grant No. 1929112. They also acknowledge the support of computational resources from the Advanced Research Computing Center (ARCC) at the University of Wyoming. The work by D. D. Fong was supported by the U.S. Department of Energy (DOE), Office of Science, Basic Energy Sciences (BES), Materials Sciences and Engineering Division. The authors declare no competing financial interests.

DATA AVAILABILITY

The data that support the findings of this study are available from the corresponding author upon reasonable request.

REFERENCES

[1]J. Jiang, D. G. Lim, K. Ramadoss, and S. Ramanathan, "Ionic conduction and unipolar resistance switching in δ-phase Bi_2O_3 thin films," Solid-State Electron. **146**, 13–20 (2018).
[2]N. M. Sammes, G. A. Tompsett, H. Näfe, and F. Aldinger, "Bismuth based oxide electrolytes—Structure and ionic conductivity," J. Eur. Ceram. Soc. **19**, 1801–1826 (1999).
[3]D. S. Aidhy, R. Sachan, E. Zarkadoula, O. Pakarinen, M. F. Chisholm, Y. Zhang, and W. J. Weber, "Fast ion conductivity in strained defect-fluorite structure created by ion tracks in $Gd_2Ti_2O_7$," Sci. Rep. **5**(1), 16297 (2015).
[4]I. C. Tung, G. Luo, J. H. Lee, S. H. Chang, J. Moyer, H. Hong, M. J. Bedzyk, H. Zhou, D. Morgan, D. D. Fong, and J. W. Freeland, "Polarity-driven oxygen vacancy formation in ultrathin $LaNiO_3$ films on $SrTiO_3$," Phys. Rev. Mater. **1**(5), 053404 (2017).
[5]M. Golalikhani, Q. Lei, R. U. Chandrasena, L. Kasaei, H. Park, J. Bai, P. Orgiani, J. Ciston, G. E. Sterbinsky, D. A. Arena, P. Shafer, E. Arenholz, B. A. Davidson, A. J. Millis, A. X. Gray, and X. X. Xi, "Nature of the metal-insulator transition in few-unit-cell-thick $LaNiO_3$ films," Nat. Commun. **9**(1), 2206 (2018).
[6]W. J. Weber and R. C. Ewing, "Plutonium immobilization and radiation effects," Science **289**, 2051–2052 (2000).

[7]K. E. Sickafus, L. Minervini, R. W. Grimes, J. A. Valdez, M. Ishimaru, F. Li, K. J. McClellan, and T. Hartmann, "Radiation tolerance of complex oxides," Science **289**, 748–751 (2000).
[8]K. E. Sickafus, R. W. Grimes, J. A. Valdez, A. Cleave, M. Tang, M. Ishimaru, S. M. Corish, C. R. Stanek, and B. P. Uberuaga, "Radiation-induced amorphization resistance and radiation tolerance in structurally related oxides," Nat. Mater. **6**, 217–223 (2007).
[9]D. S. Aidhy, B. Liu, Y. Zhang, and W. J. Weber, "Chemical expansion affected oxygen vacancy stability in different oxide structures from first principles calculations," Comput. Mater. Sci. **99**, 298–305 (2015).
[10]S. V. Kalinin and N. A. Spaldin, "Functional ion defects in transition metal oxides," Science **341**, 858–859 (2013).
[11]Y. M. Kim, J. He, M. D. Biegalski, H. Ambaye, V. Lauter, H. M. Christen, S. T. Pantelides, S. J. Pennycook, S. V. Kalinin, and A. Y. Borisevich, "Probing oxygen vacancy concentration and homogeneity in solid-oxide fuel-cell cathode materials on the subunit-cell level," Nat. Mater. **11**, 888–894 (2012).
[12]N. Jiang and E. D. Wachsman, "Structural stability and conductivity of phase-stabilized cubic bismuth oxides," J. Am. Ceram. Soc. **82**, 3057–3064 (1999).
[13]D. S. Aidhy, S. B. Sinnott, E. D. Wachsman, S. R. Phillpot, and J. C. Nino, "Structure of δ-Bi_2O_3 from density functional theory: A systematic crystallographic analysis," J. Solid State Chem. **182**, 1222–1228 (2009).
[14]P. L. Popa, S. Sønderby, S. Kerdsongpanya, J. Lu, H. Arwin, and P. Eklund, "Structural, morphological, and optical properties of Bi_2O_3 thin films grown by reactive sputtering," Thin Solid Films **624**, 41–48 (2017).
[15]S. H. Jung, E. D. Wachsman, and N. Jiang, "Structural stability and conductivity of cubic $(WO_3)_{x}$. $(Dy_2O_3)_{y}$.$(Bi_2O_3)_{1-x-y}$," Ionics **8**, 210–214 (2002).
[16]S. Durmuş, V. Çorumlu, T. Çifci, I. Ermis, and M. Arı, "Electrical, structural and thermal properties of nanoceramic $(Bi_2O_3)_{1-x-y}(Ho_2O_3)_x(Tm_2O_3)_y$ ternary system," Ceram. Int. **39**, 5241–5246 (2013).
[17]R. D. Sánchez, M. T. Causa, A. Caneiro, A. Butera, M. Vallet-Regí, M. J. Sayagués, J. González-Calbet, F. García-Sanz, and J. Rivas, "Metal-insulator transition in oxygen-deficient $LaNiO_{3-x}$ perovskites," Phys. Rev. B **54**, 16574–16578 (1996).
[18]R. Jaramillo, S. D. Ha, D. M. Silevitch, and S. Ramanathan, "Origins of bad-metal conductivity and the insulator–metal transition in the rare-earth nickelates," Nat. Phys. **10**, 304–307 (2014).
[19]M. Pirzada, R. W. Grimes, L. Minervini, J. F. Maguire, and K. E. Sickafus, "Oxygen migration in $A_2B_2O_7$ pyrochlores," Solid State Ionics **140**, 201–208 (2001).
[20]D. G. Schlom, L.-Q. Chen, C. J. Fennie, V. Gopalan, D. A. Muller, X. Pan, R. Ramesh, and R. Uecker, "Elastic strain engineering of ferroic oxides," MRS Bull. **39**, 118–130 (2014).
[21]D. Li, K. Lee, B. Y. Wang, M. Osada, S. Crossley, H. R. Lee, Y. Cui, Y. Hikita, and H. Y. Hwang, "Superconductivity in an infinite-layer nickelate," Nature **572**, 624–627 (2019).
[22]M.-B. Lepetit, B. Mercey, and C. Simon, "Interface effects in perovskite thin films," Phys. Rev. Lett. **108**, 087202 (2012).
[23]M. Ziese, H. C. Semmelhack, and K. H. Han, "Strain-induced orbital ordering in thin $La_{0.7}Ca_{0.3}MnO_3$ films on $SrTiO_3$," Phys. Rev. B **68**, 134444 (2003).
[24]J. Garcia-Barriocanal, A. Rivera-Calzada, M. Varela, Z. Sefrioui, E. Iborra, C. Leon, S. J. Pennycook, and J. Santamaria, "Colossal ionic conductivity at interfaces of epitaxial ZrO_2:Y_2O_3/$SrTiO_3$ heterostructures," Science **321**, 676–680 (2008).
[25]R. A. De Souza, A. Ramadan, and S. Hörner, "Modifying the barriers for oxygen-vacancy migration in fluorite-structured CeO_2 electrolytes through strain: A computer simulation study," Energy Environ. Sci. **5**, 5445–5453 (2012).
[26]D. S. Aidhy, B. Liu, Y. Zhang, and W. J. Weber, "Strain-induced phase and oxygen-vacancy stability in ionic interfaces from first-principles calculations," J. Phys. Chem. C **118**, 30139–30144 (2014).
[27]U. Aschauer, R. Pfenninger, S. M. Selbach, T. Grande, and N. A. Spaldin, "Strain-controlled oxygen vacancy formation and ordering in $CaMnO_3$," Phys. Rev. B **88**, 054111 (2013).
[28]U. Aschauer, N. Vonrüti, and N. A. Spaldin, "Effect of epitaxial strain on cation and anion vacancy formation in MnO," Phys. Rev. B **92**, 054103 (2015).
[29]W. Donner, C. Chen, M. Liu, A. J. Jacobson, Y.-L. Lee, M. Gadre, and D. Morgan, "Epitaxial strain-induced chemical ordering in $La_{0.5}Sr_{0.5}CoO_{3-\delta}$ films on $SrTiO_3$," Chem. Mater. **23**, 984–988 (2011).
[30]K. Ahn, Y.-C. Chung, K. J. Yoon, J.-W. Son, B.-K. Kim, H.-W. Lee, and J.-H. Lee, "Lattice-strain effect on oxygen vacancy formation in gadolinium-doped ceria," J. Electroceram. **32**, 72–77 (2014).
[31]C. Cazorla, "Lattice effects on the formation of oxygen vacancies in perovskite thin films," Phys. Rev. Appl. **7**, 044025 (2017).
[32]J. J. Plata, A. M. Márquez, and J. F. Sanz, "Understanding the interplay of dopants, interfaces, and anionic conductivity in doped ceria/zirconia heteroepitaxial structures," Chem. Mater. **26**, 3385–3390 (2014).
[33]D. S. Aidhy, J. C. Nino, S. B. Sinnott, E. D. Wachsman, and S. R. Phillpot, "Vacancy-ordered structure of cubic bismuth oxide from simulation and crystallographic analysis," J. Am. Ceram. Soc. **91**, 2349–2356 (2008).
[34]S. Boyapati, E. D. Wachsman, and N. Jiang, "Effect of oxygen sublattice ordering on interstitial transport mechanism and conductivity activation energies in phase-stabilized cubic bismuth oxides," Solid State Ionics **140**, 149–160 (2001).
[35]A. Malashevich and S. Ismail-Beigi, "First-principles study of oxygen-deficient $LaNiO_3$ structures," Phys. Rev. B **92**, 144102 (2015).
[36]M. Toshihiro, U. Osamu, I. Tomomi, N. Ichiro, M. Ichiro, K. Tsuneo, K. Shinichi, and K. Fumikazu, "Synthesis, crystal structure, and properties of oxygen-deficient lanthanum nickelate $LaNiO_{3-x}$ $(0 \leq x \leq 0.5)$," Bull. Chem. Soc. Jpn. **67**, 687–693 (1994).
[37]B. Berini, N. Keller, Y. Dumont, E. Popova, W. Noun, and M. Guyot, "Reversible phase transformation of $LaNiO_{3-x}$ thin films studied *in situ* by spectroscopic ellipsometry," Phys. Rev. B **76**, 205417 (2007).
[38]J. M. Gonzalez-Calbet, M. J. Sayagues, and M. Vallet-Regi, "An electron diffraction study of new phases in the $LaNiO_{3-x}$ system," Solid State Ionics **32–33**, 721–726 (1989).
[39]G. Kresse and J. Furthmüller, "Efficient iterative schemes for ab initio total-energy calculations using a plane-wave basis set," Phys. Rev. B **54**, 11169–11186 (1996).
[40]J. P. Perdew, K. Burke, and M. Ernzerhof, "Generalized gradient approximation made simple," Phys. Rev. Lett. **77**, 3865–3868 (1996).
[41]H. J. Monkhorst and J. D. Pack, "Special points for brillouin-zone integrations," Phys. Rev. B **13**, 5188–5192 (1976).
[42]S. J. May, J. W. Kim, J. M. Rondinelli, E. Karapetrova, N. A. Spaldin, A. Bhattacharya, and P. J. Ryan, "Quantifying octahedral rotations in strained perovskite oxide films," Phys. Rev. B **82**, 014110 (2010).
[43]S. Plimpton, "Fast parallel algorithms for short-range molecular dynamics," J. Comput. Phys. **117**, 1–19 (1995). http://lammps.sandia.gov.
[44]P. W. M. Jacobs and D. A. Mac Donaill, "Computational simulations of delta-Bi_2O_3. 1. Disorder," Solid State Ionics **23**, 279–293 (1987).
[45]A. Kushima and B. Yildiz, "Oxygen ion diffusivity in strained yttria stabilized zirconia: Where is the fastest strain?," J. Mater. Chem. **20**, 4809–4819 (2010).
[46]D. S. Aidhy, Y. Zhang, and W. J. Weber, "Strained ionic interfaces: Effect on oxygen diffusivity from atomistic simulations," J. Phys. Chem. C **118**, 4207–4212 (2014).
[47]D. S. Aidhy, "Oxygen diffusion in ThO_2-CeO_2 and ThO_2-UO_2 solid solutions from atomistic calculations," Phys. Chem. Chem. Phys. **18**, 15019–15024 (2016).
[48]D. S. Aidhy and W. J. Weber, "Microstructure design for fast oxygen conduction," J. Mater. Res. **31**, 2–16 (2016).
[49]M. Kubicek, Z. Cai, W. Ma, B. Yildiz, H. Hutter, and J. Fleig, "Tensile lattice strain accelerates oxygen surface exchange and diffusion in $La_{(1-x)}Sr_{(x)}CoO_{(3-x)}$ thin films," ACS Nano **7**, 3276–3286 (2013).
[50]B. Yildiz, "'Stretching' the energy landscape of oxides—Effects on electrocatalysis and diffusion," MRS Bull. **39**, 147–156 (2014).
[51]K. Hirai, R. Aso, Y. Ozaki, D. Kan, M. Haruta, N. Ichikawa, H. Kurata, and Y. Shimakawa, "Melting of oxygen vacancy order at oxide–heterostructure interface," ACS Appl. Mater. Interfaces **9**, 30143–30148 (2017).
[52]D. Marrocchelli, S. R. Bishop, H. L. Tuller, and B. Yildiz, "Understanding chemical expansion in non-stoichiometric oxides: Ceria and zirconia case studies," Adv. Funct. Mater. **22**, 1958–1965 (2012).

[53]D. Marrocchelli, S. R. Bishop, H. L. Tuller, G. W. Watson, and B. Yildiz, "Charge localization increases chemical expansion in cerium-based oxide," Phys. Chem. Chem. Phys. **14**, 12070–12074 (2012).
[54]W. C. Yang, Y. T. Xie, W. K. Zhu, K. Park, A. P. Chen, Y. Losovyj, Z. Li, H. M. Liu, M. Starr, J. A. Acosta, C. G. Tao, N. Li, Q. X. Jia, J. J. Heremans, and S. X. Zhang, "Epitaxial thin films of pyrochlore iridate $Bi_{2+x}Ir_{2-y}O_{7-\delta}$: Structure, defects and transport properties," Sci. Rep. **7**, 7740 (2017).
[55]B. Scrosati, A. Magistris, C. M. Mari, and G. Mariotto, *Fast Ion Transport in Solids* (Springer, 1993), p. 272.
[56]A. Laarif and F. Theobald, "The lone pair concept and the conductivity of bismuth oxides Bi_2O_3," Solid State Ionics **21**, 183–193 (1986).
[57]M. Nord, P. E. Vullum, M. Moreau, J. E. Boschker, S. M. Selbach, R. Holmestad, and T. Tybell, "Structural phases driven by oxygen vacancies at the $La_{0.7}Sr_{0.3}MnO_3$/$SrTiO_3$ hetero-interface," Appl. Phys. Lett. **106**, 041604 (2015).
[58]K. Barry, B. Zhang, N. Anand, Y. Xin, A. Vailionis, J. Neu, C. Heikes, C. Cochran, H. Zhou, Y. Qiu, W. Ratcliff, T. Siegrist, and C. Beekman, "Modification of spin-ice physics in $Ho_2Ti_2O_7$ thin films," Phys. Rev. Mater. **3**, 084412 (2019).